

# Comparison of Continuous and Pulsed Wave Lasers in Keyhole Welding of Stainless-Steel to Aluminium

Julio Coroado (✉ [julio.coroado@gmail.com](mailto:julio.coroado@gmail.com))

Cranfield University

Supriyo Ganguly

Cranfield University

Stewart Williams

Cranfield University

Wojciech Suder

Cranfield University

Sonia Meco

Cranfield University

Goncalo Pardal

Cranfield University

---

## Research Article

**Keywords:** dissimilar metal joining, keyhole laser welding, intermetallic compounds, aluminium, stainless-steel.

**Posted Date:** August 4th, 2021

**DOI:** <https://doi.org/10.21203/rs.3.rs-683158/v1>

**License:**  This work is licensed under a Creative Commons Attribution 4.0 International License.

[Read Full License](#)

---

**Version of Record:** A version of this preprint was published at The International Journal of Advanced Manufacturing Technology on October 31st, 2021. See the published version at <https://doi.org/10.1007/s00170-021-08226-5>.

# **Comparison of continuous and pulsed wave lasers in keyhole welding of stainless-steel to aluminium**

**Julio Coroado\*<sup>1</sup>, Supriyo Ganguly<sup>1</sup>, Stewart Williams<sup>1</sup>, Wojciech Suder<sup>1</sup>, Sonia Meco<sup>1</sup>, Goncalo Pardal<sup>1</sup>**

*<sup>1</sup> Welding Engineering and Laser Processing Centre, Cranfield University, Cranfield  
MK43 0AL, UK*

## **Abstract**

A continuous wave (CW) and a nanosecond pulsed wave (PW) lasers were used to join 1 mm thick sheets of SS304L (SS) austenitic stainless-steel to AA5251 (Al) aluminium alloy in an overlap joint configuration. The weld shape (penetration depth and width), intermetallic compounds concentration, weld quality (cracking and porosity) and mechanical strength were correlated with the process energy and compared between each laser temporal mode. Successful CW joints were produced with the SS sheet on top of the Al, but the opposite configuration revealed to be impossible for the range of parameters tested. The PW joints were successful with the Al sheet on top of SS, but all the joints cracked at the interface when the opposite configuration was used. The mechanical tests showed that even though it is possible to achieve higher tensile shear load in CW welds due to the larger bonding area, the load per unit of weld length revealed to be almost 5x higher for PW welds at similar applied energy.

**Keywords:** dissimilar metal joining, keyhole laser welding, intermetallic compounds, aluminium, stainless-steel.

\*Corresponding author. Tel.: +447438093485.

E-mail address: julio.coroado@gmail.com (J. Coroado)

## **1.0 Introduction**

Dissimilar joining of SS to Al alloys is widely used in thin gauge materials in aerospace and automotive applications, seeking to improve the fuel efficiency through weight reduction. The combination of lightweight of Al alloys and the good corrosion resistance and weldability of SS alloys bring higher quality and economic demand where several material requirements are desired for similar applications, such as electric vehicles (EVs) battery enclosure/housings which contain large number of cells [1]. However, due to the different physical properties and chemical incompatibility of the alloys, the joining process becomes challenging [2]. The low solid solubility of Al into iron (Fe) and the almost zero solid solubility of iron into aluminium is responsible for the formation of brittle intermetallic compounds (IMCs). The presence of the IMCs added to the differences in melting point, thermal expansion coefficient, thermal conductivity and specific heat capacity may lead to the formation of brittle intermetallic compounds (IMCs) and consequently defects such as cracking, causing brittle failure in service due to internal stresses after fusion welding [3]. The IMCs formed have different crystal structures in comparison to the base metals. Solid Fe and molten Al reaction is controlled by diffusion [4]. When

temperature on the SS side approaches the Al melting temperature, the diffusion coefficient of Fe into Al increases, but the opposite is not verified if SS is still solid.

Temperature and time are the key parameters in the formation and growth of the IMCs [4][5]. It is not possible to control them independently in order to minimize the amount of IMCs and maximise the mechanical strength of joints produced, as low heat input leads to less IMCs but also smaller welds and lower strength. Mechanical joining processes such as screwing, riveting, roll bonding or clinching are good alternatives since no IMCs are formed [6][7]. More recently, friction stir welding, a solid state joining process, was also successfully employed, avoiding fully molten material [8]. Nevertheless, tool wear and lack of flexibility in the joint geometry are some of the limitations. On the other hand, some fusion based joining processes such as resistance spot welding and laser-MIG hybrid welding create a large weld pool due to the long thermal cycle, which enhances the IMCs formation [9].

Laser welding is a popular process to join dissimilar materials. Localized energy input of the welding source allows a minimal heat affected zone. The high cooling rates and short processing time compared with other techniques reduces diffusion of Fe in Al and thus, the formation of Fe-Al ( $\text{Fe}_3\text{Al}$ ,  $\text{FeAl}_2$ ,  $\text{Fe}_2\text{Al}_3$ ,  $\text{Fe}_2\text{Al}_5$ ,  $\text{FeAl}_3$ ) [10][11] and Al-Cr ( $\text{Al}_4\text{Cr}$ ,  $\text{Al}_8\text{Cr}_5$ ,  $\text{Al}_9\text{Cr}_4$ ) binary compounds commonly formed at the joint interface [12]. As an industrially commonly used joining technique, laser welding can be employed in welding applications in automotive battery packs where laser is used to precisely join small cylindrical cells ( $\leq 0.5$  mm thick) but also large cells with geometrical large interconnectors [1]. Another prominent application associated is

the manufacturing of biomedical devices, orthopaedic and prosthetic implants which require in some cases several microscopic welds to join thin materials ( $\leq 1$  mm thick) [13].

There are two types of laser temporal modes: CW and PW. The PW lasers have lower average power but higher peak power on each pulse, leading to high power density and deep keyhole, being able to create narrow weld profiles with high aspect ratio [14]. The higher peak power promotes more vaporisation than CW laser for the same average power, which associated to a rapid energy application within a short duration allows fast material solidification, being better for dissimilar metal joining. Many researchers used lasers to weld dissimilar materials. Huang et al. [15] studied the formation of brittle IMCs using high energy and a high repetition femtosecond laser to join Al to SS ( $\leq 1$  mm thick). The formation of IMCs was restricted, and crack formation suppressed due to highly localized heat generation, which minimized the heat input into the material. Yang et al. [16] joined pure Al and SS (0.8 mm thick) using a millisecond PW laser. They found that for deeper welds, hard Al rich IMCs were formed, which deteriorated the strength of the joint. Many micro-cracks were observed in the Al-rich IMCs, and almost no defects were discovered in the Fe-rich IMCs at the joint interface. The two previous studies suggest that different pulse durations can be used to successfully reduce the IMCs formation. However, the results were analysed in terms of system parameters, being difficult the comparison of both lasers to understand how the Al-rich IMCs should be avoided independently of the laser used. Nanosecond PW lasers can also be used to enhance the joining of 1 mm thick Al to 0.85 mm thick steel sheet [17]. Defect free Fe-Al joints were

achieved by laser spot welding using laser-textured steel: first, the surface of steel was textured using a nanosecond PW laser and then, the spot welding process was performed with a defocused and stationary CW laser. The steel plate was positioned on top of the Al sheet with a texture faced down to the Al surface in a lap-joint configuration. The results suggested that the maximum tensile-shear load was improved due to an increase in the bonding area created by the textured surface and the quality and uniformity of the weld nuggets. Nevertheless, several weld spots or different weld patterns could also have been used to improve the bonding area.

CW laser can also be used for dissimilar welds with good results. Meco et al. [18] successfully minimized the reaction between Fe and Al by joining steel to Al in a lap-joint configuration operating a CW laser in conduction mode. This technique also allowed successful T-joints produced by melting the Al plate, which was inserted into a steel plate [19]. In a different study, Meco et al. [20] used a FE model to predict the thermal cycle at the interface between steel and Al plates using different laser parameters. They showed that a small bonding area is equally detrimental to the mechanical strength of the joint as having a thick IMC layer. The FE model suggested that temperature to which the materials are exposed is more critical than the time, as this is the factor with higher contribution to the growth of the IMC layer and the formation of the bonding area. Power density was found to be the dominant parameter controlling the peak temperature. Hence, this parameter should be low in order to avoid high temperatures and consequently brittle IMCs at the joint interface. It is important to note that since the previous studies were performed in terms of power density, interaction time and energy, the results can be equally and easily

compared to any other CW laser. Sierra et al. [21] showed that when Al was placed upon steel, the IMC layer created by a CW laser was larger when compared to the opposite configuration. This was caused due to the increased diffusion of Fe into molten Al when the steel plate was still solid. The high concentration of hard and brittle  $\text{Fe}_2\text{Al}_5$  in the Al interface was detrimental to the strength of the welds [21][22].

The advancements of the latest generation of fibre pulsed lasers in pulse shape modulation, higher peak powers and shorter pulse durations available can bring advantages in minimizing the IMC concentration through a fast freezing of the melt pool. Nevertheless, their lower average power in comparison to CW lasers can be a major drawback for the application in thicker material sheets. The previous studies showed that is possible to achieve good joints between SS and Al using PW and CW lasers, but the results are case to case sensitive. However, it wasn't found any direct comparison between both laser temporal modes in order to quantify which one offers better control of the IMCs at the joint interface, better weld shape flexibility to increase the bonding area and consequently stronger joints. Therefore, it is necessary a like-for-like comparison of both lasers with a systematic and controlled way to achieve large enough joints without overheating the materials.

The aim of this research is to compare continuous wave and pulsed wave in order to understand how the bond area, weld shape, IMCs distribution and lap-joint configuration affect the mechanical strength of welds achieved at similar applied energy per unit length.

## 2.0 Definition of the fundamental laser material interaction parameters

To enable like for like comparison between CW and PW lasers, a concept of fundamental laser material interaction parameters (FLMIP) has been used this work [23][24][25]. These parameters fully describe the laser-material interaction, allowing the replication of similar weld shapes in different laser systems operated in CW mode [23][24] and PW mode [25] because they control the weld thermal cycle [26].

The application of energy per unit length on the material is well defined for CW mode. However, as shown in Fig. 1, in nano-second PW seam welding the energy is delivered in the form of individual pulses or trains of pulses with a characteristic pulse energy ( $E_{\text{pulse}}$ ), peak power and pulse duration ( $P_{\text{width}}$ ). Since the peak power is only instantaneous, similarly to previous studies [27][28], this work has also considered the average peak power for pulse energy calculation purposes.

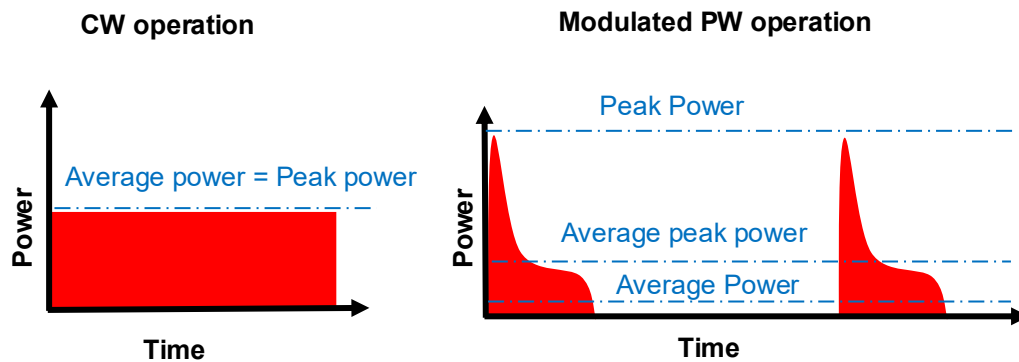


**Fig. 1 Differentiation of lasers in terms of temporal outputs in continuous wave and modulated pulsed wave mode [29]**

In CW mode, the process can be specified using power density ( $q_p$ ), interaction time ( $t_i$ ) and specific point energy ( $E_{\text{SP}}$ ), as given by Eqs. (1-3) [26]. The first one is

determined as the ratio of the laser average power ( $P_L$ ) to the area of laser spot on the material's surface ( $A_s$ ), which for a circular beam diameter is given by Eq. (1). The interaction time is defined as the ratio of the beam diameter ( $d$ ) in the welding direction to the travel speed ( $v$ ), given by Eq. (2). The energy delivered to any specific point on the weld centreline is equal to the product of power density, interaction time and the area of the laser spot on the surface, as given by Eq. (3).

$$q_p = \frac{P_L}{A_s} [MW/cm^2] \quad (1)$$

$$t_i = \frac{d}{v} [ms] \quad (2)$$

$$E_{SP} = q_p * t_i * A_s = P_L * t_i [J] \quad (3)$$

The output characterization of the nano-second PW laser used in this work is shown in Fig. 2. Each temporal mode, referred to as waveform, has optimum pulse repetition frequency ( $PRF_0$ ) where the average peak power ( $P_{peak}$ ) and pulse energy are maximum. Above  $PRF_0$ , the average power remains constant but the pulse energy and average peak power are reduced, whereas below  $PRF_0$ , the average power decreases but the average peak power and pulse energy remain constant [30], as given by Eq. (4) and Eq. (5), respectively. The duty cycle has different limits depending on the average peak power selected. The percentage of overlap between consecutive spots is given by Eq. (6) [31].

$$P_{peak} = E_{pulse} / P_{width} [W] \quad (4)$$

$$E_{pulse} = P_L / PRF [J] \quad (5)$$

$$O_F = \left(1 - \frac{v}{d * PRF}\right) * 100 \text{ [%]} \quad (6)$$

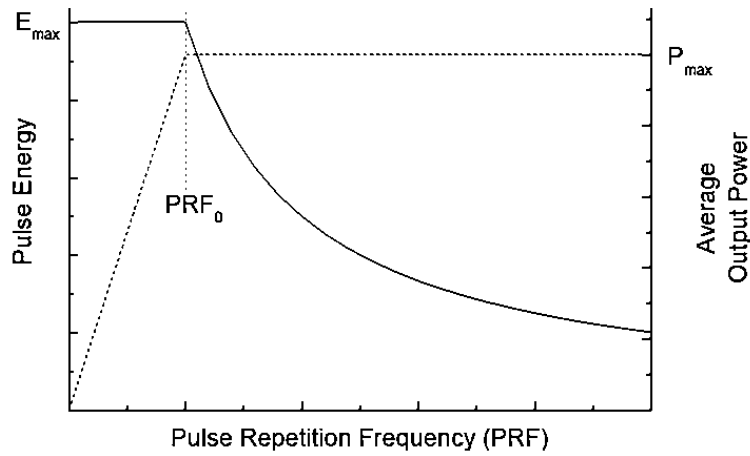


**Fig. 2 Output characterization of the nano-second PW laser [27]**

The analysis of the PW welding results was also made using FLMIP: However, in PW mode the interaction time defines the time in which a point is exposed to the laser beam in the weld centreline. It is dependent on the duration of each pulse and the overlap between them, as given by Eq. (7). At 0% overlap factor, the interaction time is equal to pulse width and at 100% the equation is not applicable, since the beam is stationary. Hence, Eq. (7) is only applicable below 100% of overlapping factor [17]. As previously explained in Fig. 2,  $P_{peak}$  change with PRF for constant average power. Therefore, the average peak power density ( $q_{p, peak}$ ) in Eq. (8) is defined by the ratio of  $P_{peak}$  by the area of the laser spot, whereas the specific pulse energy ( $E_{SP, pulse}$ ) in Eq.(9) represents the overall energy delivered by several pulses for a certain laser-material interaction time.

$$t_i = \left( \frac{P_{width}}{1 - \frac{O_f}{100}} \right) [ms] \quad (7)$$

$$q_{p, peak} = \frac{P_{peak}}{A_s} [MW/cm^2] \quad (8)$$

$$E_{SP, pulse} = q_{p, peak} * t_i * A_s = P_{peak} * t_i [J] \quad (9)$$

### 3.0 Experimental set-up

The welds were carried out in 1 mm thick 5251 Al alloy and 304L austenitic SS. The chemical composition of each alloy is shown in Table 1. The physical and mechanical properties are shown in Table 2.

**Table 1 Chemical composition of the base materials [32][33]**

Material	Elements (wt.%)													
	Si	Fe	P	Cu	Mn	Mg	N	Ni	Zn	Ti	Cr	C	Al	Fe
<b>5251</b>	Max	Max	-	Max	0.1	1.7	-	-	Max	Max	Max	-	Bal.	-
<b>H22</b>	0.4	0.5	-	0.15	-	-	-	-	0.15	0.15	0.15	-	Bal.	-
<b>304 L</b>	Max 1.00	Bal.	Max 0.05	-	Max 2.00	-	Max 0.11	8.00 – 10.50	-	-	17.50 - 19.50	Max 0.03	-	Bal.

**Table 2 Physical and mechanical properties of the base materials [32][33][34]**

Property	Symbol	Units	Al 5251 H22	SS304L
Density	$\rho$	g/cm <sup>3</sup>	2.69	8.0
Melting Temperature	$T_m$	K	898	1723
Vaporisation Temperature	$T_v$	W.(m.K) <sup>-1</sup>	2790	3023
Thermal conductivity average	k	W m <sup>-1</sup> K <sup>-1</sup>	134	16.2
Latent heat of melting	$H_m$	J.kg <sup>-1</sup>	3.5 x 10 <sup>5</sup>	2.73 x 10 <sup>5</sup>
Latent heat of vaporisation	$H_v$	J.kg <sup>-1</sup>	1.19 x 10 <sup>7</sup>	6.1 x 10 <sup>6</sup>
Thermal diffusivity average	$\alpha$	m <sup>2</sup> s <sup>-1</sup>	5.7 x 10 <sup>-5</sup>	5.5 x 10 <sup>-5</sup>
Specific heat of solid phase	$c_{ps}$	J.kg <sup>-1</sup> .K <sup>-1</sup>	850	477
Viscosity	$\eta$	m.Pas	1.3	8
Modulus of Elasticity	E	GPa	70	193
Proof Stress	$\delta$	MPa	120 min	220 min
Tensile Strength	UTS	MPa	190 - 230	520 - 700

The welding configuration used, and corresponding dimensions are shown in Fig 3. Lap-joints were performed positioning SS on top of Al (SS-Al) and vice-versa (Al-SS). According to the literature survey, the IMC grow with temperature and time. A

copper heat sink can efficiently extract the heat away from the joint due to its high thermal conductivity [4]. By reducing the thermal cycle, the growth of the IMCs but also the likelihood of distortion are reduced [35]. Therefore, a 5 mm thick copper backing bar was used. The welding tests were carried out with two different SPI fibre lasers independently used: a 500W average power CW fibre laser and a 100W average power nano-second pulsed fibre laser. The power of both lasers was measured and calibrated by a Laserpoint power meter and the beam profiles were measured using a DataRay slit scan beam profiler, showing both Gaussian beam profiles. The 35  $\mu\text{m}$  beam diameters of both lasers was focused using the same 160 mm f-theta focusing lens connected to a Galvanometer-scanner. An air-knife was used with compressed gas to protect the lens from spatter and no shielding gas was applied on the substrate. Before welding, the base materials were ground to remove the oxide layer and residues and then cleaned with acetone.

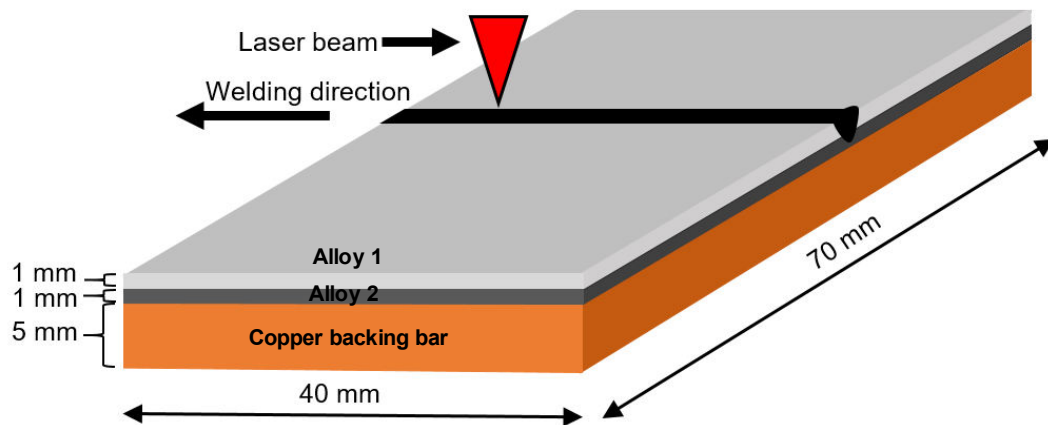


**Fig 3 Lap-joints dimensions of SS-Al and Al-SS**

## 4.0 Methodology

### 4.1 CW laser welding of SS-Al and Al-SS

This section aims to investigate the influence of power density ( $q_p$ ) and specific point energy ( $E_{SP}$ ) in the bonding quality of lap welded joints of SS-Al and Al-SS, using a CW laser. For a constant beam diameter of 35  $\mu\text{m}$ , different combinations of average power and travel speed were used, resulting in a range of  $q_p$  from 26 to 49  $\text{MW}/\text{cm}^2$  and  $E_{SP}$  from 137 to 1000  $\text{mJ}$ , according to Eqs. (1) and (3), respectively. The set of parameters used, and the respective results of the bonding success are shown in Table 3. The values presented result from a number of experiments produced to identify the necessary laser parameters to ensure successful bonding between the base materials.

**Table 3 CW laser welding parameters and results for a beam diameter of 35  $\mu\text{m}$**

System Parameters			FLMIP		
Beam diameter [ $\mu\text{m}$ ]	Average Power [W]	Travel Speed [mm/s]	Interaction time [ms]	Average Power Density [ $\text{MW}/\text{cm}^2$ ]	Specific Point Energy [mJ]
d	$P_L$	v	$t_i$	$q_p$	$E_{SP}$
35	250-472	11-94	0.40-3.2	26-49	137-100

### 4.2 PW laser welding of SS-Al and Al-SS

A nanosecond PW laser was used to join SS-Al and Al-SS. The aim is to study the influence of average peak power density ( $q_{p, \text{peak}}$ ) and specific pulse energy ( $E_{SP, \text{pulse}}$ ) in the bonding quality of lap-joints and compare the processing parameters to achieve similar PW and CW welds. Only one waveform with maximum pulse energy and longest pulse duration available in the laser has been selected. Its

characteristics are shown in Table 4. For a constant beam diameter of 35  $\mu\text{m}$ , average power of 100 W and pulse width of 500 ns, different combinations of peak power, pulse energy, travel speed and pulse repetition frequency were used, resulting in a constant  $q_p$  of 10.4  $\text{MW}/\text{cm}^2$  and a range of  $q_{p, \text{peak}}$  from 33 to 208  $\text{MW}/\text{cm}^2$  and  $E_{\text{SP, pulse}}$  from 250 to 1000 mJ, according to Eqs. (1), (8) and (9), respectively. The set of parameters used are shown in Table 5.

**Table 4 Characteristics of waveform 31 of PW laser**

Waveform	PRF0 (kHz)	Max pulse energy, $E_{\text{max}}$ (mJ)	Pulse width (ns)	Peak Power at $E_{\text{max}}$ (kW)
31	100	1	500	7

**Table 5 PW laser welding parameters for a beam diameter of 35  $\mu\text{m}$ , average power of 100 W and pulse width of 500 ns**

System parameters			Calculated parameters			FLMIP			
Frequency (kHz)	Travel speed (mm/s)	Pulse energy (mJ)	Peak power (kW)	Overlap factor (%)	Duty cycle (%)	Average power density ( $\text{MW}/\text{cm}^2$ )	Average peak power density ( $\text{MW}/\text{cm}^2$ )	Specific pulse energy (mJ)	Interaction time (ms)
PRF	$v$	$E_{\text{Pulse}}$	$P_{\text{peak}}$	$\theta_F$	DC	$q_p$	$q_{p, \text{peak}}$	$E_{\text{SP, pulse}}$	$t_i$
100 - 807	3.5 - 14	0.12 - 1.0	0.25 - 2.0	99.9-99.98	5 - 40.4	10.4	26-208	250-1000	0.5-3.2

### 4.3 Mechanical strength characterisation

Tensile shear tests were carried out to analyse the mechanical strength of selected successful joints from Table 3 and Table 5 for CW and PW mode, respectively. The maximum load and maximum load per unit of length of the welds were compared between both laser processing modes for similar applied energies. The ultimate

tensile strength (UTS) was also calculated for the strongest joint achieved in each mode by dividing the maximum load by the area of the weld cross-section. The tests were performed at room temperature using an electromechanical Instron 5500 machine, with a load cell of 3 kN and a crosshead displacement of 0.5 mm/min perpendicular to the weld direction. The geometry and dimensions of the cross weld lap tensile-shear test specimens were compliant with ISO 14273:2001 standards for mechanical tensile shear testing of seam welds [36]. Fig. 4 shows the weld line patterns used for the tensile testing. The test sample was straight lined, 25 mm wide and 160 mm long. Different number of 25 mm long horizontal weld line patterns were used: (a) single line, (b) 2 lines and (c) 4 lines, separated by 5 mm each. The elongation of the parent metals was measured using a laser extensometer model LE-15, for a gauge length of 30 mm.

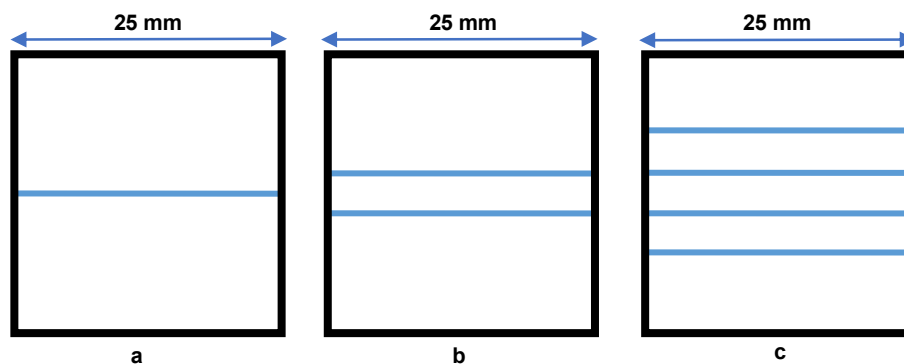


**Fig. 4 Pattern of weld lines used for tensile testing**

#### **4.4 Metallographic characterization**

The cross sections were mounted in plastic moulds using an epoxy resin mixed with a hardener, ground and then polished to mirror like surface. The microstructure of

aluminium was revealed by etching its surface with Keller’s reagent, whereas stainless-steel was electrolytically etched with 10% of oxalic acid. Micrographs were taken with an Optiphot optical microscope with several magnification levels. A scanning electron microscope (SEM) equipment was also used to investigate the composition and distribution of the IMC on the fusion zone of the welds with an integrated energy-dispersive X-ray spectroscopy (EDS).

## 5.0 Results and discussion

### 5.1 CW laser welding of SS-Al and Al-SS

The CW laser was used to join SS-Al in the first stage and then, in a second stage, Al-SS. The welding parameters used are shown in Table 6.

**Table 6 Laser welding parameters and results for a beam diameter of 35  $\mu\text{m}$**

System Parameters			FLMIP			Successful bonding?	
Beam diameter [ $\mu\text{m}$ ]	Average Power [W]	Travel Speed [mm/s]	Interaction time [ms]	Average Power Density [MW/cm <sup>2</sup> ]	Specific Point Energy [mJ]	SS-Al lap-joint	Al-SS lap-joint
d	P <sub>L</sub>	v	t <sub>i</sub>	q <sub>p</sub>	E <sub>SP</sub>	-	-
35	250	64	0.55	26	137	NO	NO
35	250	32	1.1	26	273	YES	NO
35	250	16	2.2	26	545	YES	NO
35	304	64	0.55	32	166	NO	NO
35	304	32	1.1	32	333	YES	NO
35	304	16	2.2	32	665	YES	NO
35	320	64	0.50	33	176	YES	NO
35	320	41	0.90	33	273	YES	NO
35	320	34	1.0	33	333	YES	NO
35	320	22	1.6	33	516	YES	NO
35	320	11	3.2	33	1000	YES	NO
35	472	94	0.40	49	176	YES	NO
35	472	64	0.50	49	258	YES	NO
35	472	32	1.1	49	516	NO	NO

It is shown in Fig 5a-c the fusion zone of the lap-joints of SS-Al for different levels of specific point energy and constant power density. In Fig 5d-f, it is shown in more detail the respective joints magnification from Fig 5a-c. Due to the lower vaporisation temperature of Al in comparison to stainless-steel (Table 2), in Fig 5a occurred a violent ejection of metal for the highest  $E_{SP}$  and  $q_p$  applied. As  $E_{SP}$  decreased from Fig 5d-f at constant  $q_p$  through a reduction in  $t_i$  (Table 6), the penetration depth decreased as well and weld quality was improved, i.e. cracks were reduced. This improvement is related with the IMC formation, since they are dependent on the time and temperature of the process, decreasing with a reduction in energy input [35]. It is important to highlight the difficulty in achieving low energy levels with CW lasers, since high travel speeds are required to achieve rapid melting and solidification and consequently, low IMC formation.

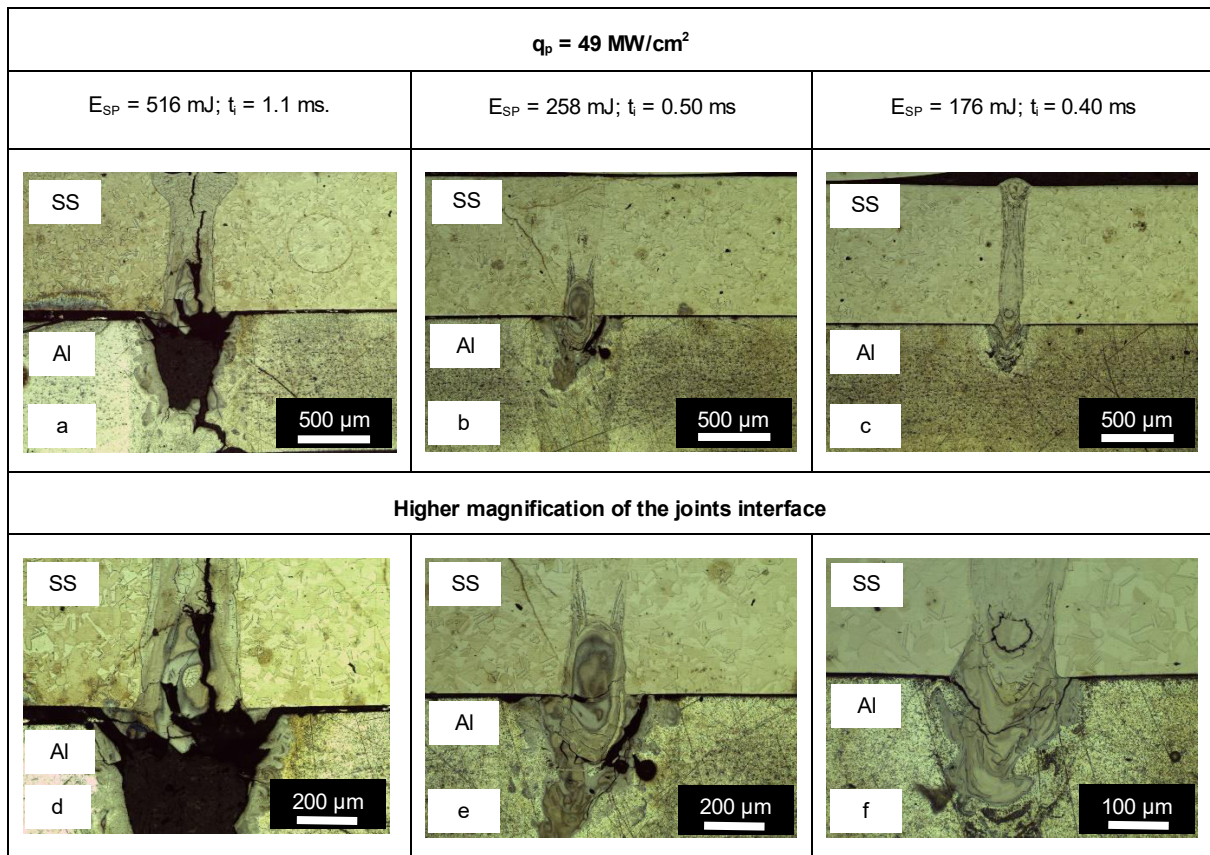


**Fig 5 CW lap-joints of SS-Al for constant  $q_p$  of  $49 \text{ MW/cm}^2$  and different  $E_{SP}$  and  $t_i$**

In Fig 5, the IMC were mixed and not distributed in a thin layer as a needle shape along the interface, as observed in previous studies for laser conduction mode [35][37][38]. Since this study has been performed in keyhole mode, the mixing of both alloys was enhanced and the IMCs distributed around the fusion zone, as observed in the EDS mapping in Fig. 6. A several times lower viscosity of Al as compared to SS (Table 2) must be considered as an important factor to explain how easy Fe diffuses in Al, enhancing their mixing. Moreover, the higher density of SS in comparison to Al (Table 2) may also have facilitated the mixing of both alloys. A similar explanation was given by Lee et al. when they tried to join Al to copper [39].

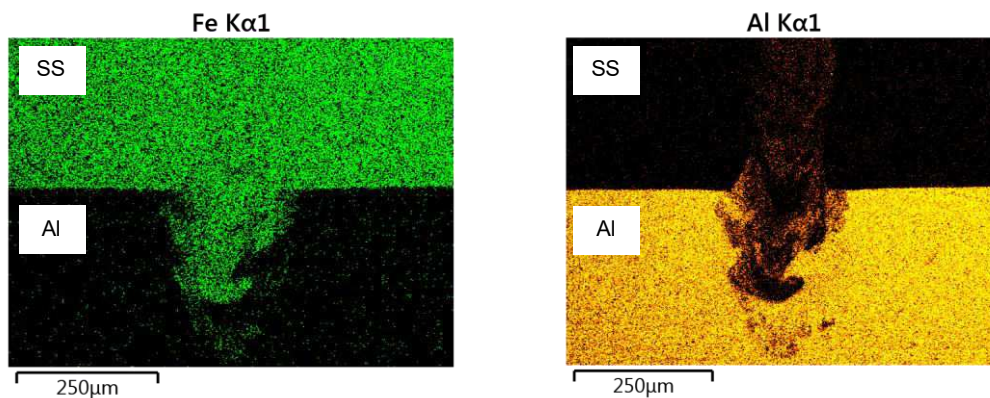


**Fig. 6 EDS mapping of Fe and Al elements from a CW lap-joint of SS-Al for  $q_p$  of  $49 \text{ MW/cm}^2$ ,  $E_{SP}$  of  $176 \text{ mJ}$  and  $t_i$  of  $0.4 \text{ ms}$**

It is known that lower power density decreases the reaction rate between Al and Fe, enabling a better control of the IMCs formation [35]. Therefore, in this work, the power density has been decreased from  $49 \text{ MW/cm}^2$  in Fig 5 to  $33 \text{ MW/cm}^2$  in Fig. 7 at constant  $E_{SP}$  through a reduction in average power and travel speed (Table 6). As expected, the weld quality has been improved, despite the small cracks caused by the remaining IMCs. Some solute bands of Fe-Al phases are visible on the edge of the weld. These bands have also been observed by Sierra et al. when joining steel to Al using a high-power CW laser [21]. They attributed their origin to the upward convection movements occurring at high temperature, entrapping Al in steel. A rise in the volume of liquid Al due to the increase of steel penetration led to a greater Al–Fe dilution, which resulted in thicker bands, as observed in Fig. 7d. These bands could form: (1) locally richer aluminium Fe–Al alloys, (2)  $\text{Fe}_x\text{Al}_y$  intermetallic phases if the formation threshold had been reached, or (3) could solidify as pure Al. [21].

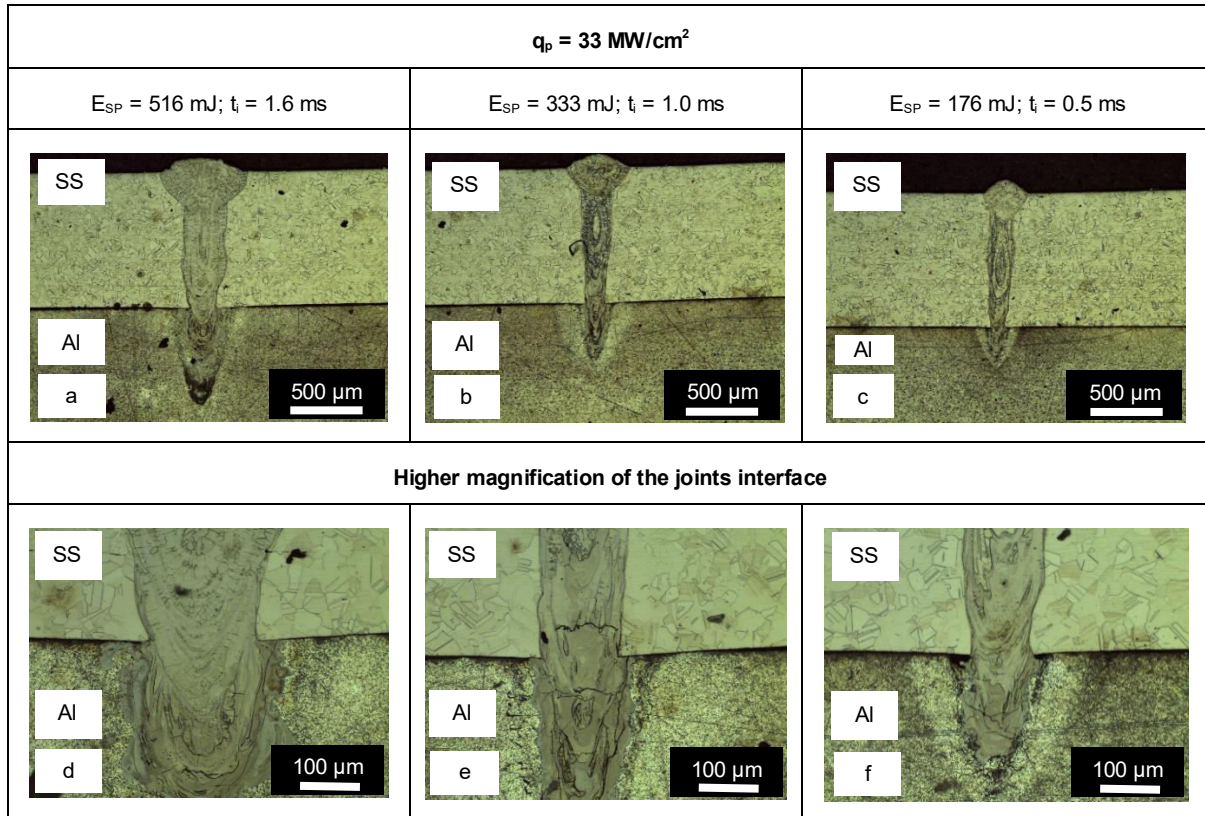


**Fig. 7 CW lap-joints of SS-Al for constant  $q_p$  of  $33 \text{ MW/cm}^2$  and different  $E_{SP}$  and  $t_i$**

The IMCs distribution from Fig. 7f was analysed in EDS spectrums in Fig 8. Spectrum number 34 shows that, in the stainless-steel sheet, there is a small concentration of Al and no cracks are visible in this region. At spectrum number 37, the concentration of Al increased slightly, and the cracks formation is more evident. Moving further into Al to spectrum number 38, the atomic percentage of Al is even higher and very similar to Fe, which coincides with the increase of the size of the cracks. However, due to the scattered intermetallic compounds, close to the edge of the joint interface on spectrum number 43, the atomic percentage of Al is also high, and a small crack is visible. This is because the high peak temperature generated by

the high-power density applied in a small beam, resulted in a rise in the recoil pressure, causing an upward convection of Al [27].

The IMCs are organized into two groups, the Fe-rich and the Al-rich IMCs. The hardest and thus more brittle IMCs are found in the Al-rich group [40][38] for an atomic concentration (at) of Al above 58%. Sierra et al. [21] observed that the hardness and consequently, the cracks formation, increased in steel-on-aluminium laser welds for deeper penetrations, mainly attributed to an increase in Al ratio in the weld. These conclusions are in agreement with spectrum 34 from Fig 8b, where the at.% of Al is below 10% and no cracks are visible, being all the Al dissolved in Fe [40][38], and also with spectrum 38, where the at.% of Al is close to 40% and larger cracks can be observed. However, due to the severe Al gradients across the weld metal area, different IMCs could have been formed on specific locations.

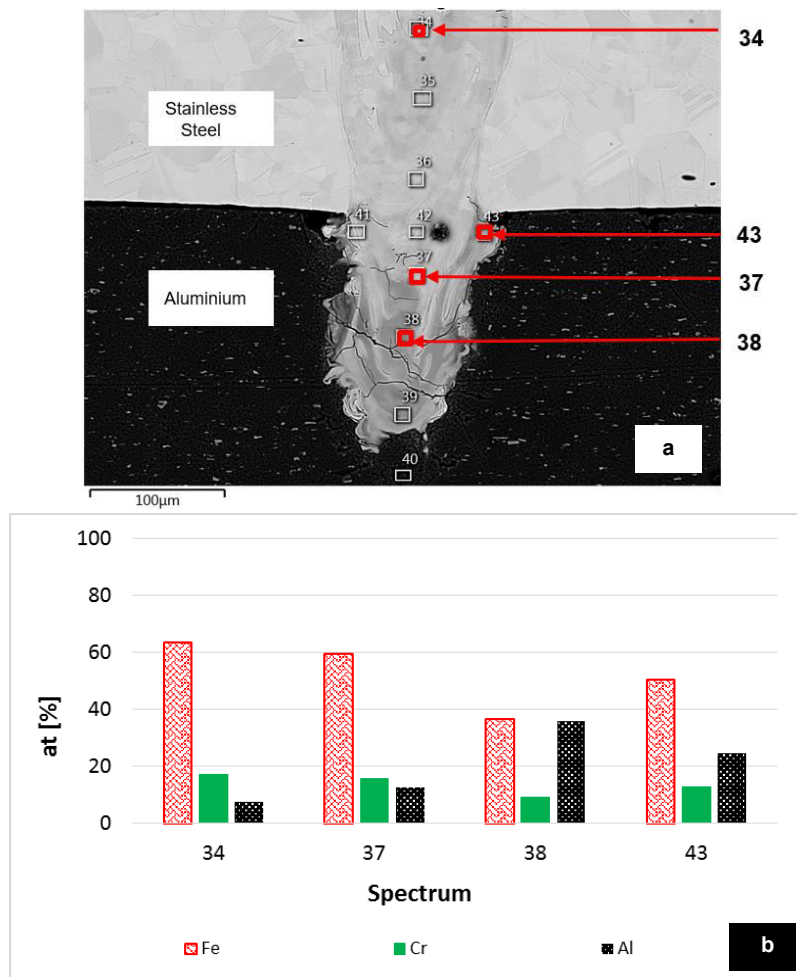


**Fig 8 SEM micrograph (a) and respective EDS spectrum analysis (b) from a CW lap-joint of SS-Al for  $q_p$  of 33 MW/cm<sup>2</sup>,  $E_{SP}$  of 176 mJ and  $t_i$  of 0.5 ms**

The welding parameters from Fig. 7 were replicated for a Al-SS lap-joint configuration and presented in Fig. 9. Despite the reduction of  $E_{SP}$  at constant  $q_p$  from Fig. 9a-c, no successful lap-joints were possible to achieve, breaking at the interface. In Fig. 9a (Al-SS), for specific point energy of 516 mJ and power density of 33 MW/cm<sup>2</sup>, the weld width of the upper sheet of Al was greater as in comparison to Fig. 7a (SS-Al). The higher thermal conductivity by a factor of eight and lower melting temperature by a factor of two of Al (Table 2), allowed to create a larger

fusion zone in Fig. 9a, conducting the heat faster to SS. On the other hand, for SS-Al in Fig. 7a, similar energy of 516 mJ took longer to reach the Al sheet for a similar interaction time of 0.5 ms, since the specific heat capacity of SS is 1.8x lower than Al. Thus, the peak temperature reached at the joint interface was lower, decreasing the penetration depth and the IMCs concentration in comparison to the Al-SS lap-joint in Fig. 9a. This may explain difference in bonding for both joint configurations. Similar results were observed by Sierra et al. when joining aluminium-on-steel [21]. All welds performed were cracked at the joint interface. The steel interface exhibited large IMCs, more than 50  $\mu\text{m}$  thick because the liquid was richer in steel. They concluded that the cracks were probably related to the sensitivity to hot cracking of the Al alloys used in their study.

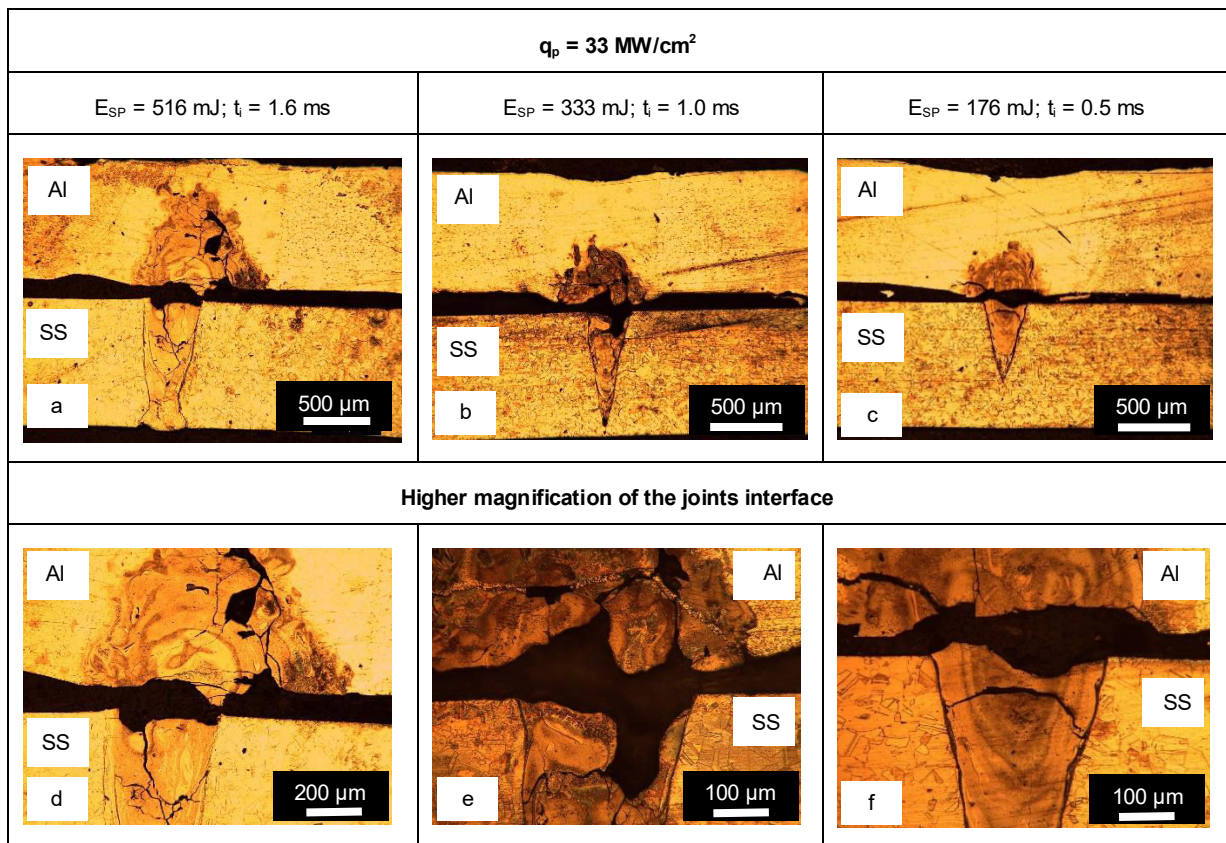


**Fig. 9 CW lap-joints of Al-SS for constant  $q_p$  of  $33 \text{ MW/cm}^2$  and different  $E_{SP}$  and  $t_i$**

## 5.2 PW laser welding of SS-Al and Al-SS

In this section, a PW laser was used to join SS-Al in the first stage and then Al-SS in a second stage. The welding parameters used are shown in Table 7.

**Table 7 PW laser welding parameters and results for a beam diameter of 35  $\mu\text{m}$ , average power of 100 W and pulse width of 500 ns.**

System parameters			Calculated parameters			FLMIP				Successful bonding?	
Frequency (kHz)	Travel speed (mm/s)	Pulse energy (mJ)	Peak power (kW)	Overlap factor (%)	Duty cycle (%)	Average power density ( $\text{MW}/\text{cm}^2$ )	Average peak power density ( $\text{MW}/\text{cm}^2$ )	Specific pulse energy (mJ)	Interaction time (ms)	SS-Al lap-joint	Al-SS lap-joint
PRF	v	$E_{\text{Pulse}}$	$P_{\text{peak}}$	$O_F$	DC	$q_p$	$q_{p, \text{peak}}$	$E_{\text{SP, pulse}}$	$t_i$	-	-
100	3.5	1.0	2.0	99.9	5	10.4	208	1000	0.5	NO	YES
150	5.2	0.67	1.3	99.9	7.5	10.4	139	667	0.5	NO	YES
300	10.5	0.33	0.67	99.9	15	10.4	69	333	0.5	NO	YES
400	14	0.25	0.50	99.9	20	10.4	52	250	0.5	NO	NO
807	6.4	0.12	0.25	99.98	40.4	10.4	26	545	2.2	NO	NO
640	3.5	0.16	0.31	99.98	32	10.4	33	1000	3.2	NO	NO
426	6.8	0.23	0.47	99.96	21.3	10.4	49	516	1.1	NO	NO

In Fig. 10a is shown a PW lap-joint of SS-Al for  $q_{p, \text{peak}}$  of  $208 \text{ MW}/\text{cm}^2$  and  $E_{\text{SP, pulse}}$  of 1000 mJ. The respective EDS spectrum analysis is shown Fig. 10b. Several voids can be observed along the fusion zone in Fig. 10a. Magnesium is one of the main alloying elements of the Al alloy used in this study (Table 1). Since the vaporisation temperature of magnesium (1363 K) is much lower than SS (3023 K) and Al (2790 K), its vaporisation may have a strong contribution for the keyhole instability, increasing the capillary forces generated and the defects likelihood in the weld pool [28][41]. The lower viscosity of Al as compared to SS also enables more efficient melt removal from the bottom of the keyhole [34].

The EDS spectrum analysis from Fig. 10b indicates a high concentration of Fe in the centre of the SS sheet, being residual the atomic percentage of Al. However, on the edge of the same horizontal line, the atomic percentage of Al is 49%. On the Al sheet, in the middle of the fusion zone the atomic percentage of Al is almost 100%. The presence of voids caused by the entrapment of the vaporised alloys after solidification enhanced the mixing of both metals at the interface [42] where the atomic percentage of Al is above 70%. For these Al percentages,  $F_2Al_5$  and  $FeAl_3$  phases were formed [12][40][38]. The low fracture toughness of each phase may explain the lack of bonding between these alloys for the parameters tested due to crack formation [42].

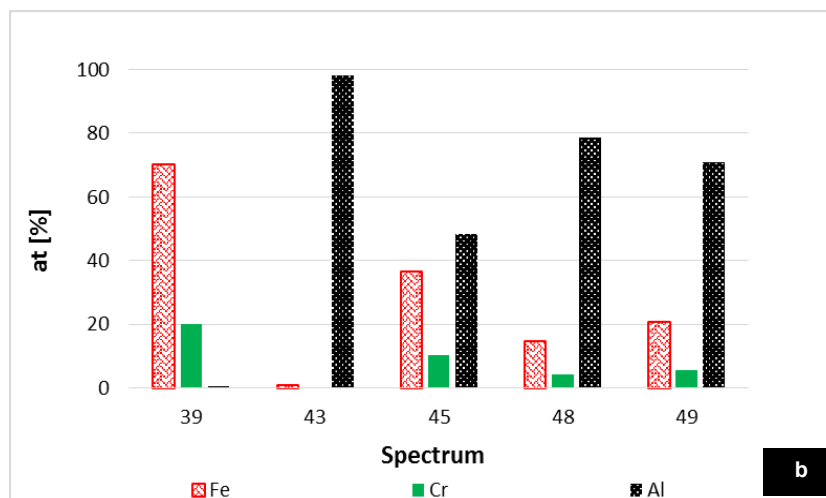
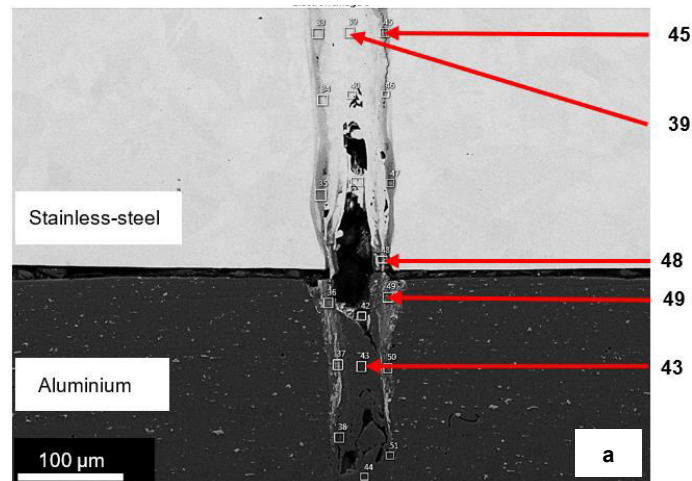


**Fig. 10 SEM micrograph (a) and respective EDS spectrum analysis (b) from a PW lap-joint of SS-Al for  $q_p$  of  $10.4 \text{ MW/cm}^2$ ,  $q_{p, \text{peak}}$  of  $208 \text{ MW/cm}^2$ ,  $E_{\text{SP, pulse}}$  of  $1000 \text{ mJ}$  and  $t_i$  of  $0.5 \text{ ms}$**

The SS-Al lap-joints were unsuccessful using a PW laser, but successful in CW mode, as demonstrated in the previous section. A comparison between both temporal modes is shown in Fig. 11 for similar penetration depth of 1.2 mm. Despite the lower average power of the PW laser in comparison to the CW laser, its higher peak power generated a higher average peak power density applied in Fig. 11b, increasing the vaporisation of Al and its alloying elements. This is likely to cause the

escape of the vaporised elements towards the top of the narrow weld, causing a high pressure at the joint interface by a descending stream of molten steel and an ascending stream of molten Al, enhancing the mixing between the base metals and the formation of brittle IMCs. Moreover, the difference in thermal expansion coefficient of both alloys [3] will force a gap between both sheets, cracking the narrow joint, avoiding the bonding. However, this phenomenon is not so evident in CW mode in Fig. 11a. For a similar interaction time of 0.5 ms, CW laser utilizes a duty cycle of 100% at a travel speed of 64 mm/s (Table 6), whereas with PW laser a duty cycle of 15% and a travel speed of 10.5 mm/s are applied. Thus, the thermal losses are lower in CW mode than in PW mode, being possible to achieve similar penetration depth and a larger weld width at lower applied energy. Due to the deeper depth of penetration, a greater volume of SS was mixed in Al, breaking the balance between recoil pressure and surface tension, enhancing the mixing between both alloys at the bottom of the weld, as previously shown in the EDS mapping from Fig 8. Hence, in CW mode, most of the brittle IMCs concentration are shifted away from the joint interface, improving the bonding between both alloys.

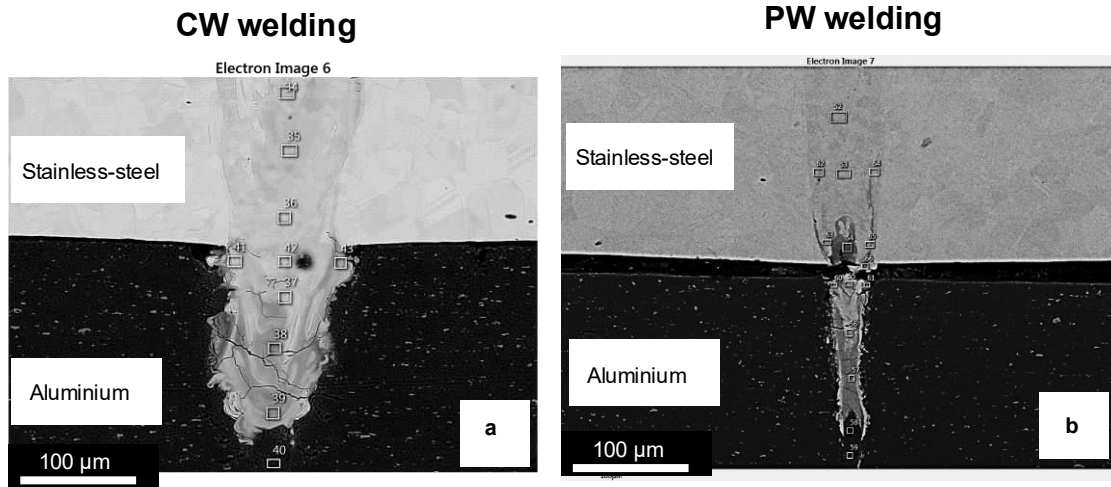


**Fig. 11 SS-Al lap-joints for a penetration depth of 1.2 mm: (a) CW welding at  $q_p$  of 33 MW/cm<sup>2</sup>,  $E_{SP}$  of 176 mJ and  $t_i$  of 0.5 ms; (b) PW welding at  $q_p$  of 10.4 MW/cm<sup>2</sup>,  $q_{p, peak}$  of 69 MW/cm<sup>2</sup>,  $E_{SP, pulse}$  of 333 mJ and  $t_i$  of 0.5 ms**

The welding parameters from Table 5 have been replicated for Al-SS lap-joint configuration and presented in Fig. 12. Decreasing  $E_{SP, pulse}$  and  $q_{p, peak}$  at constant  $q_p$  and  $t_i$  through an increase in travel speed and PRF, the penetration depth decreased from Fig. 12a-c and the weld quality was decreased as well, with some cracks being visible at the joint interface in Fig. 12f. Due to Al positioned on top, its alloying elements are more likely to vaporise and escape from the top of the weld pool, generating capillary forces which drag SS (Fe) into Al, as observed in the EDS mapping from Fig. 13, corresponding to Fig. 12d. Similar results were observed in Fig. 9 for CW mode.

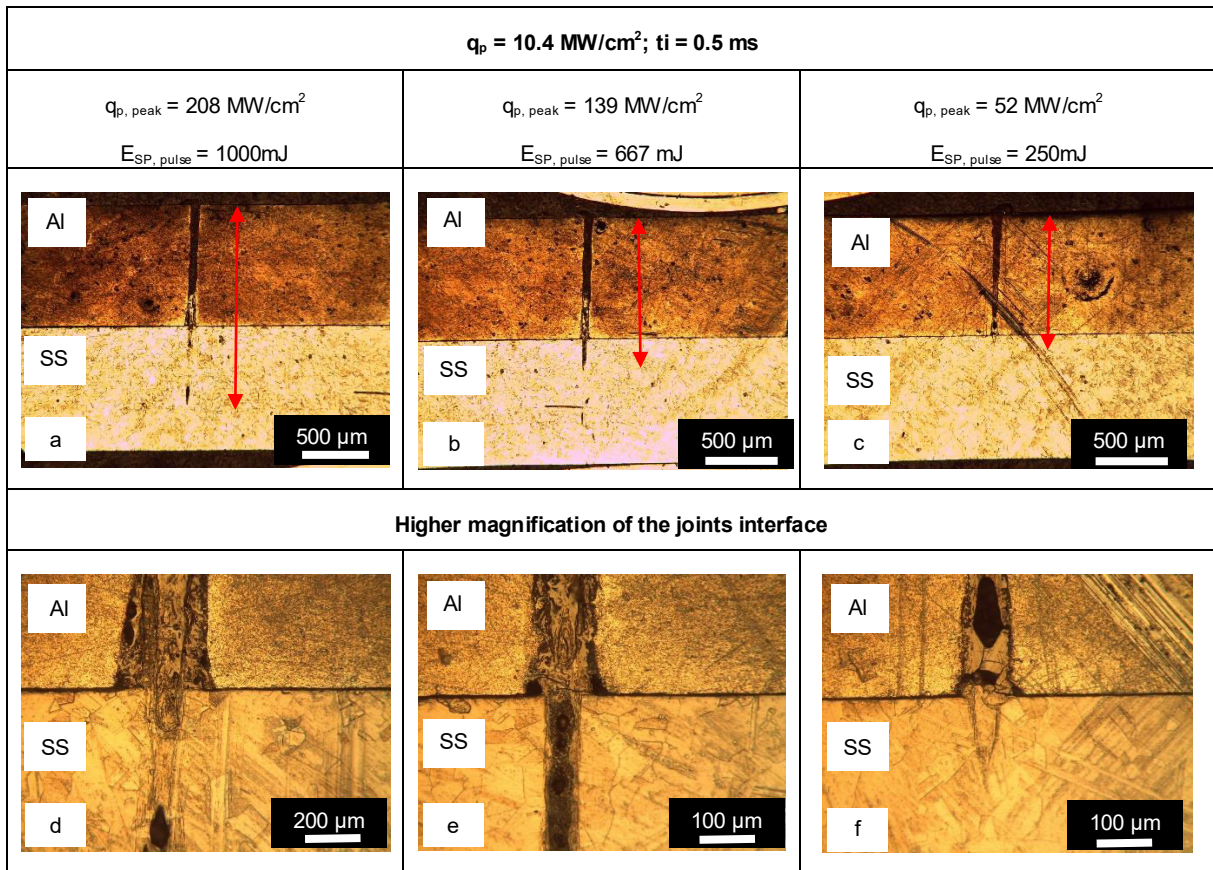


**Fig. 12 PW lap-joints of Al-SS for constant  $q_p$  of 10.4,  $t_i$  of 0.5 ms and different  $q_{p, \text{ peak}}$  and  $E_{SP, \text{ pulse}}$**

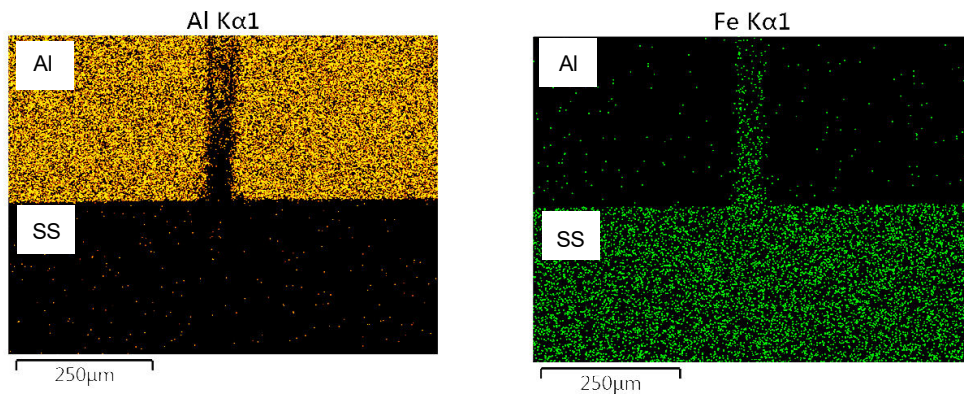


**Fig. 13 EDS mapping of Fe and Al elements from a PW lap-joint of Al-SS for  $q_p$  of 10.4  $\text{MW/cm}^2$ ,  $q_{p, \text{ peak}}$  of 208  $\text{MW/cm}^2$ ,  $E_{SP, \text{ pulse}}$  of 1000 mJ and  $t_i$  of 0.5 ms**

Several sections from Fig. 12d were analysed in Fig. 14 at the top (Fig. 14a), middle (Fig. 14b) and at the joint interface (Fig. 14c). The corresponding SEM analysis is shown in Fig. 15. In spectrum 67 from Fig. 15, there is a high atomic concentration of Al in comparison to Fe, whereas in spectrum 64, the atomic percentage of iron increased. This is likely to be caused by the high peak power density applied in PW mode at a high pulse repetition frequency, which forced the stirring and mixing of Al in SS, despite the difference in density and viscosity. Consequently, the higher peak temperature in the centre of the beam increased the concentration of  $\text{FeAl}_3$  in this area, being visible a large crack along the fusion zone. In spectrum 52 from Fig. 15, the concentration of Al in the fusion zone decreased in comparison to spectrum 64, increasing the concentration of Fe, being formed FeAl phase (Iron-rich IMC), which have higher ductility [40][38]. Consequently, the cracks' size was reduced. At the joint interface, the atomic concentration of Al is almost inexistent, being dominated by iron, as shown in spectrum 39. Therefore, most of the Al is dissolved into Fe [38][40] and most of the IMCs were shifted away from this region, which is the reason why no cracks are visible.

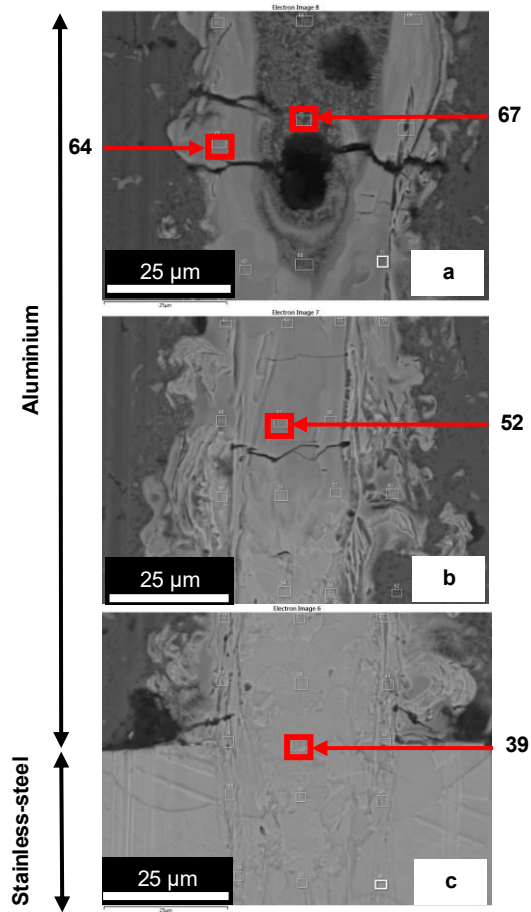


**Fig. 14 SEM micrographs from a PW lap-joint of Al-SS for  $q_p$  of  $10.4 \text{ MW/cm}^2$ ,  $q_{p, \text{ peak}}$  of  $208 \text{ MW/cm}^2$ ,  $E_{\text{SP, pulse}}$  of  $1000 \text{ mJ}$  and  $t_i$  of  $0.5 \text{ ms}$**

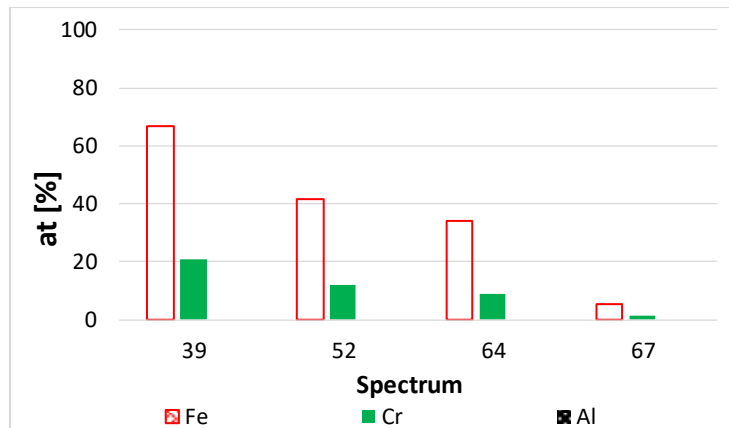


**Fig. 15 EDS spectrum analysis from a PW weld of Al-SS for  $q_p$  of  $10.4 \text{ MW/cm}^2$ ,  $q_{p, \text{ peak}}$  of  $208 \text{ MW/cm}^2$ ,  $E_{SP, \text{ pulse}}$   $1000 \text{ mJ}$  and  $t_i$  of  $0.5 \text{ ms}$**

The EDS spectrum analysis from Fig. 12f is shown in Fig 16. When the peak power density and specific pulse energy were reduced, the penetration depth and the weld quality were reduced as well, being visible more cracks on the aluminium side. The mixing between both alloys was shifted closer to the joint interface, being formed Al-rich brittle IMCs ( $\text{Fe}_2\text{Al}_3$ ) [38][40], which avoided a successful bonding. It may be possible that the reduction in the applied energy led to a reduction in peak temperature in the molten metal. Since, the temperature reduction increases the viscosity of both alloys [34], the capillary forces are reduced, being more difficult for SS to push Al towards the top of the weld pool. Hence, this may explain why the higher IMC concentration and cracks at the interface.

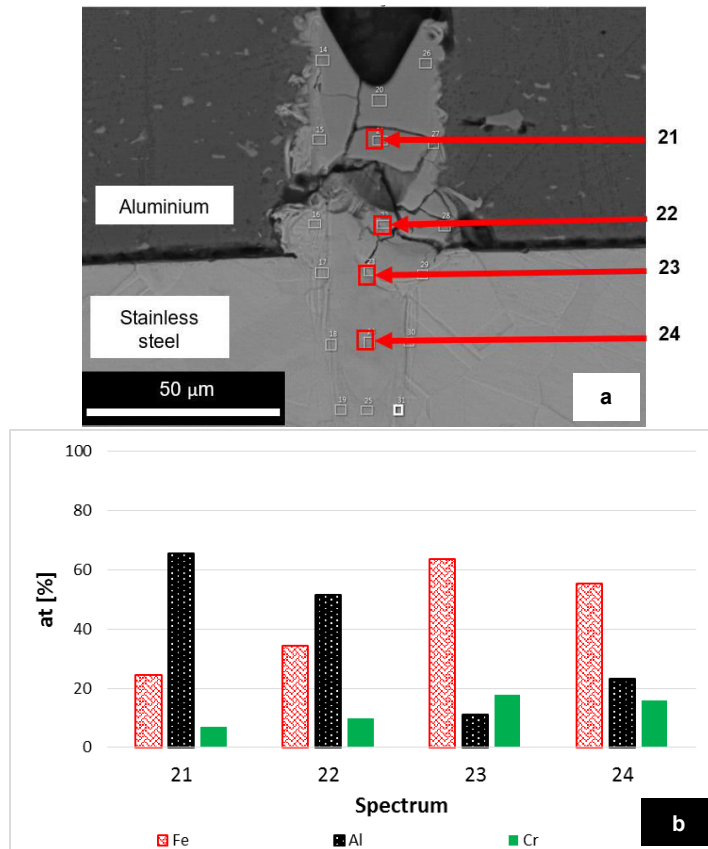


**Fig 16 SEM micrograph (a) and respective EDS spectrum analysis (b) from a PW lap-joint of Al-SS for  $q_p$  of  $10.4 \text{ MW/cm}^2$ ,  $q_{p, \text{peak}}$  of  $52 \text{ MW/cm}^2$ ,  $E_{SP, \text{pulse}}$  of  $250 \text{ mJ}$  and  $t_i$  of  $0.5 \text{ ms}$**

The lap-joints of Al-SS were successful using a PW laser, but unsuccessful in CW mode, as demonstrated in section 5.1. A comparison between both temporal modes is shown in Fig. 17 for a similar penetration depth of 1.6 mm. Due to the larger weld width of Al formed in the CW weld in Fig. 17b, iron is diffused over a larger area and the brittle IMCs are scattered along the joint interface, increasing the cracking likelihood. However, in Fig. 17a, the weld width of Al in PW mode is 10x smaller than in CW mode, forcing iron to diffuse in Al through a narrower channel, as previously

observed in the EDS mapping from Fig. 13. This phenomenon is enhanced by the faster cooling rate of the nanosecond laser in comparison to CW mode, which limits the diffusion of Al on SS for a similar interaction time of 0.5 ms. In addition to this, a smaller volume of liquid Al should minimize the mixing and prevent the IMC formation. Consequently, the mixing between both alloys in PW mode is shifted away from the joint interface, as previously shown in Fig. 14, allowing successful joints.

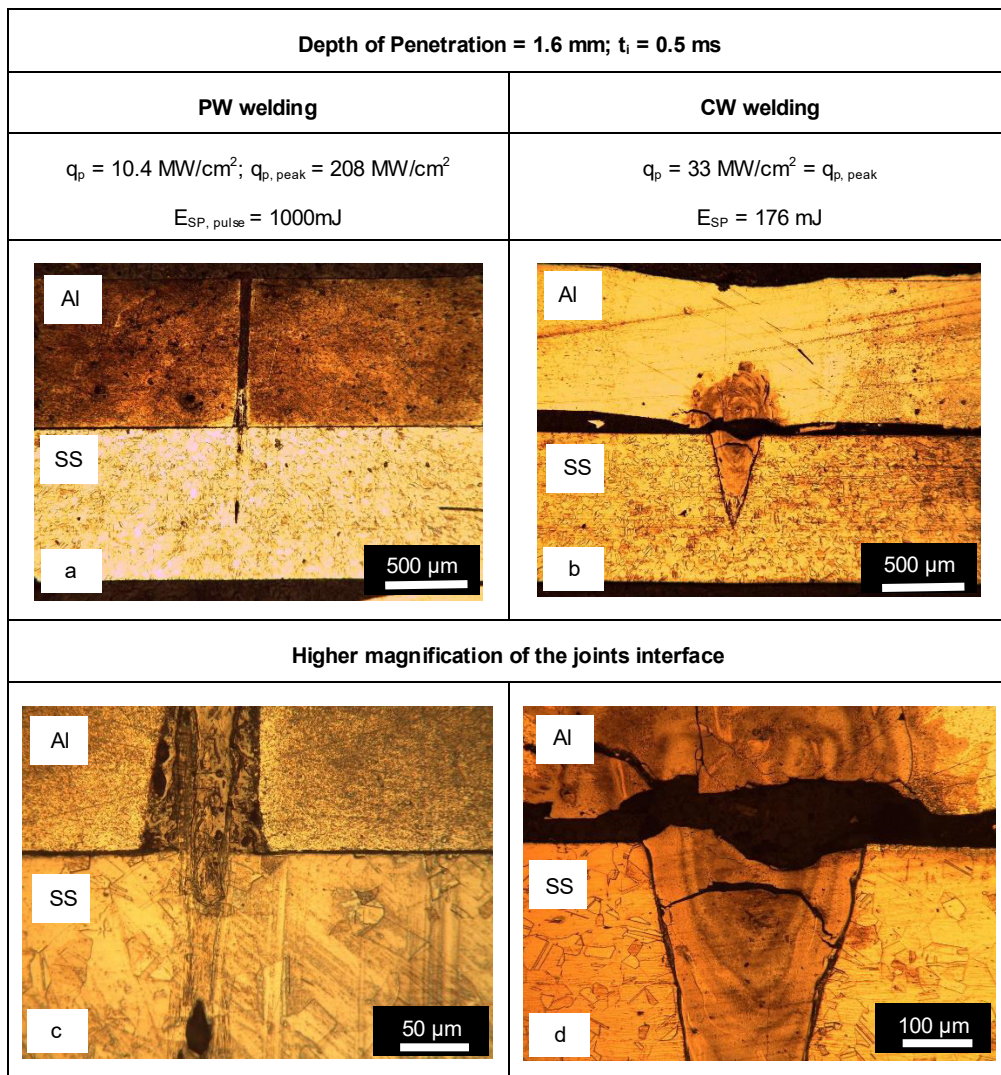


**Fig. 17 PW and CW lap-joints of Al-SS for a penetration depth of 1.6 mm and  $t_i$  of 0.5 ms**

### 5.3 Mechanical testing

#### 5.3.1 CW laser welding of SS-Al

A subsection of the successful set of parameters from Table 3 were chosen to conduct mechanical tests in order to evaluate the tensile shear load and load per unit

of weld length of CW joints. It is shown in Figure 18a that, for constant  $E_{SP}$  and  $q_p$ , the breaking load increases with an increase in the number of weld lines. There is also a trend on the increase of the tensile shear load with the increase of the energy from 333 mJ to 1000 mJ, being possible to reach 1700 N using four weld lines. This observation may be related with the larger bonding area achieved for a longer thermal cycle [20], creating a better anchoring effect of the weld-aluminium interface due to a higher penetration [21]. On the other hand, since the penetration is deeper for higher energy levels, most of the brittle IMCs are concentrated at the bottom of the weld-aluminium interface, being most of the cracks shifted away from the joint interface, reducing their propagation, as previously explained in section 5.1. Thus, the remaining cracks will avoid an increase in tensile shear load in the same proportion of the increase of weld lines number.

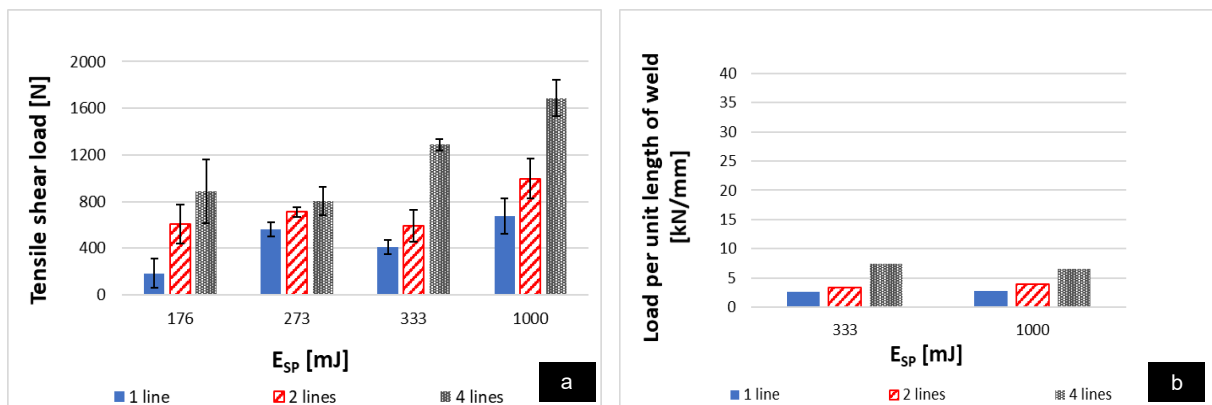


**Fig. 18 Tensile shear load and load per unit length of weld versus  $E_{SP}$  of CW lap-joints of SS-Al for  $q_p$  of 33 MW/cm<sup>2</sup>**

In Fig. 18b, the maximum load per unit length of weld was calculated by dividing the maximum tensile shear load by the weld width from Fig. 18a. As observed in Fig.

18b, by increasing  $E_{SP}$  from 333 mJ to 1000 mJ at constant  $q_p$  of 33 MW/cm<sup>2</sup>, the load remained similar for each weld pattern. Thus, the advantage of a larger bonding area for higher values of specific pulse energy may have a threshold in order to improve the load capacity, as further IMCs growth would outweigh the advantage of higher wetting area [35], decreasing the linear strength from a certain threshold [21]. These results suggest that it is difficult to further improve the mechanical strength of the joints by solely controlling the energy of the process, as also previously concluded by Meco et al. [20], but a definite answer would need more experiments. Meco et al. concluded that the bonding area is one of the key factors for the integrity of the Fe-Al joints and the mechanical strength of the joints couldn't be improved by increasing the bonding through power density since it is the parameter which most controls the temperature and consequently, the IMC growth would be enhanced. However, the authors suggested that by producing parallel weld seams, the bonding area could be increased, avoiding the negative effect of the IMCs [20]. That strategy was used in this work in Fig. 18a and has revealed to be successful.

### **5.3.2 PW laser welding of Al-SS**

The successful set of parameters from Table 5 were chosen to conduct mechanical tests and evaluate the tensile shear load and load per unit of weld length of PW joints. In Figure 19a, the maximum tensile shear load increased with the increase in the number of weld lines and with the pulse  $E_{SP}$ . A maximum load of 1330 N was achieved using four weld lines for an energy of 1000 mJ and an interaction time of 0.5 ms. For one weld line and an applied energy of 1000 mJ, the specimen

experienced a total elongation of 0.11%, slightly less when compared to the 0.14 % in CW processing. In both cases, there was some plastic deformation and the failure of all samples occurred at the metal interface.

As observed in Figure 19b, the maximum load per unit length of weld increases with  $E_{SP, pulse}$  and with the number of weld lines. However, contrary to what was observed in the previous section for CW mode, this improvement is not related with the increase of the bonding area since the PW weld width remained almost constant for different energy levels, as previously shown in Fig. 12d-f. Thus, for a constant weld width, a higher applied energy will force a larger volume of SS to push Al through a narrow channel, preventing the defects caused by the brittle IMCs at the joint interface, increasing the weld strength. The maximum tensile shear load achieved in PW mode (Figure 19a) is lower than in CW mode (Fig. 18a) for similar energy levels. Nevertheless, due to the narrower welds in PW welding, the load per unit length of weld in Figure 19b can be almost 5x higher than in CW mode in Fig. 18b. This highlights once again the importance of the higher peak power density, which allows high aspect ratio welds, and the fast freezing of the melt pool, avoiding the IMCs growth. Therefore, if the welding application requires a higher fit-up tolerance and productivity, CW laser is more indicated, providing a flexible weld shape and larger bonding areas. On the other hand, if the requirements are low heat affected zone, precise control of the heat input and narrow joints, PW is the most suitable laser.

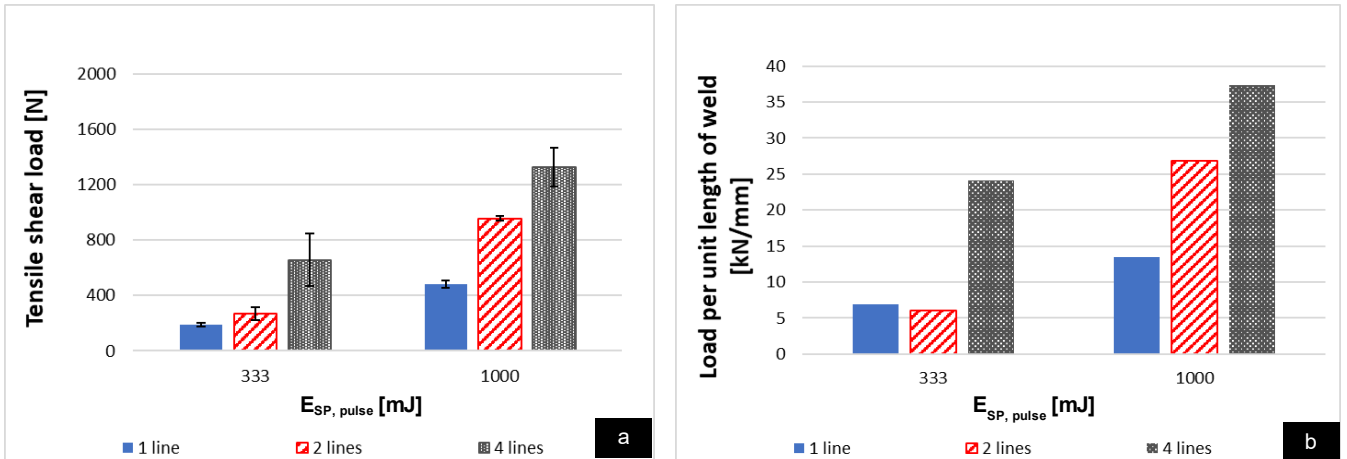


**Figure 19 Tensile shear load and load per unit length of weld versus  $E_{SP, pulse}$  of PW lap-joints of Al-SS for  $t_i$  of 0.5 ms.**

In both laser temporal modes, it was impossible to control the brittle IMCs formation for the range of parameters tested. In CW laser was harder to decouple temperature from the melt area, which created a high concentration and more scattered IMCs in the fusion zone, especially for Al-SS joints where there was a high diffusion of Fe to the wider Al weld. On the other hand, for PW laser, there was more flexibility in reducing the alloys mixing and increase the weld strength by minimizing the IMC formation through the faster freezing of the weld pool. The addition of many narrower welds using low power density and energy levels above 333 mJ allowed equivalent bonding areas to CW and localized diffusion of Fe into Al, pushing the IMCs out to the fusion zone in Al-SS joints. Thus, for similar applied energy of 1000 mJ and using four weld lines, an ultimate tensile strength (UTS) of 332 MPa was possible in Al-SS joints for PW mode, whereas in SS-Al CW welds it was only possible 65 MPa

for the same conditions. This reveals that PW welds can be nearly 5x stronger than the weakest parent metal (Al) showed in Table 2.

The limitation imposed by the melting temperature of these alloys, maximum weld width and penetration depth on the IMCs growth and distribution in the weld fusion zone, creates a limit on the laser parameters selection in order to maximise the tensile shear load. Thus, several combinations of energy and power density can be used to achieve similar welds, but the maximum load per unit length of weld can only be achieved for a certain weld shape for these alloys and thicknesses. Larger beam diameters and different weld patterns could be used to increase even more the bonding area and consequently, the weld strength. In PW mode it could also be explored shorter pulse durations in order to provide higher peak power density to push completely the IMCs out of the welding zone.

## **6.0 Conclusions**

- The SS-Al lap-joints were successful in CW mode but unsuccessful using a PW laser.
- The Al-SS lap-joints were successful using a PW laser, but unsuccessful in CW mode.
- For similar applied energy and number of weld lines, the maximum tensile shear loads were higher in CW than in PW laser welding. However, for the strongest weld, the UTS was five times higher in PW mode.

- CW laser provides better higher fit-up tolerance and productivity. On the other hand, lower heat affected zone, more precise control of the heat input and high aspect ratio welds can be achieved in PW mode.
- Further investigation using larger beam diameters and different weld patterns is recommended to increase the bonding area and consequently, the weld strength. In PW mode, different pulse durations could also be explored.

## **7.0 Declarations**

### **7.1 Compliance with Ethical Standards**

#### **7.1.1 Funding**

The researchers would like to acknowledge Innovate UK (TS/MO11089/1) for sponsoring this investigation in the scope of the Environmental Domed End project.

#### **7.1.2 Conflicts of interest/Competing interests**

The authors have no relevant financial or non-financial interests to disclose.

#### **7.1.3 Ethics approval**

To the author's knowledge, this is the first paper showing how the penetration and weld width of stainless-steel resultant from the laser welding process is controlled by the pulse power factor and interaction time. The authors confirm that this manuscript has not been published elsewhere and is not under consideration by another journal. The publication of this manuscript has also been approved by all the co-authors.

## **7.2 Consent to participate**

Not applicable.

## **7.3 Consent for publication**

The Author transfers to Springer (respective to owner if other than Springer and for U.S. government employees: to the extent transferable) the non-exclusive publication rights and he warrants that his contribution is original and that he has full power to make this grant. The author accepts responsibility for releasing this material on behalf of any and all co-authors. This transfer of publication rights covers the non-exclusive right to reproduce and distribute the article, including reprints, translations, photographic reproductions, microform, electronic form (offline, online) or any other reproductions of similar nature. The author may self-archive an author-created version of his article on his own website and his institution's repository, including his final version; however, he may not use Springer's PDF version which is posted on [www.springerlink.com](http://www.springerlink.com). Furthermore, the author may only post his version provided acknowledgement is given to the Journal and Springer as one of the original places of publication and a link is inserted to the published article on Springer's website.

## **7.4 Availability of data and material**

Not applicable.

## **7.5 Code availability**

Not applicable.

## **7.6 Authors' contributions**

- Julio Coroado – PhD student. He has designed and produced the experimental work in consultation with the other co-authors and is the principal author of the manuscript.
- Supriyo Ganguly – Reader. He helped in creation of research methodology, experimental work and provided the very essential research direction. Supriyo took active participation in preparing the manuscript.
- Stewart Williams – Professor and chair of the welding engineering and laser processing centre. He also participated actively in experimental design, data analysis and interpretation.
- Wojciech Suder – Lecturer. As one of the laser experts, Wojciech provided important knowledge on the design of the experimental work and manuscript discussion.
- Sonia Meco – Senior Research Fellow. Sonia participated in the manuscript checking and correction.
- Goncalo Pardal – Senior Research Fellow. Goncalo also took active participation in data analysis, manuscript checking and correction.

## **Acknowledgement**

The researchers would like to acknowledge Innovate UK (TS/MO11089/1) for sponsoring this investigation in the scope of the Environmental Domed End project.

## References

1. Zwicker MFR, Moghadam M, Zhang W, Nielsen CV (2020) Automotive battery pack manufacturing – a review of battery to tab joining. *J Adv Join Process* 1:100017. <https://doi.org/10.1016/j.jajp.2020.100017>
2. Springer H, Kostka A, Payton EJ, et al (2011) On the formation and growth of intermetallic phases during interdiffusion between low-carbon steel and aluminum alloys. *Acta Mater.* <https://doi.org/10.1016/j.actamat.2010.11.023>
3. Song JL, Lin SB, Yang CL, et al (2009) Spreading behavior and microstructure characteristics of dissimilar metals TIG welding-brazing of aluminum alloy to stainless steel. *Mater Sci Eng A.* <https://doi.org/10.1016/j.msea.2009.02.036>
4. Borrisutthekul R, Yachi T, Miyashita Y, Mutoh Y (2007) Suppression of intermetallic reaction layer formation by controlling heat flow in dissimilar joining of steel and aluminum alloy. *Mater Sci Eng A.* <https://doi.org/10.1016/j.msea.2007.03.049>
5. Shahverdi HR, Ghomashchi MR, Shabestari S, Hejazi J (2002) Microstructural analysis of interfacial reaction between molten aluminium and solid iron. *J Mater Process Technol.* [https://doi.org/10.1016/S0924-0136\(02\)00225-X](https://doi.org/10.1016/S0924-0136(02)00225-X)
6. Lee WB, Schmuecker M, Mercardo UA, et al (2006) Interfacial reaction in steel-aluminum joints made by friction stir welding. *Scr Mater.* <https://doi.org/10.1016/j.scriptamat.2006.04.028>
7. Soltan Ali Nezhad M, Haerian Ardakani A (2009) A study of joint quality of aluminum and low carbon steel strips by warm rolling. *Mater Des.*

<https://doi.org/10.1016/j.matdes.2008.06.042>

8. W M Thomas, D J Staines, I M Norris SAW and CSW (2006) Transition Joints Between Dissimilar Materials. TWI Ltd Granta Park Gt Abingt Cambridge CB1 6AL United Kingdom 1–7
9. Meco S, Ganguly S, Williams S, McPherson N (2014) Effect of Laser Processing Parameters on the Formation of Intermetallic Compounds in Fe-Al Dissimilar Welding. *J Mater Eng Perform* 23:3361–3370. <https://doi.org/10.1007/s11665-014-1106-5>
10. Liu XB, Pang M, Zhang ZG, et al (2007) Characteristics of deep penetration laser welding of dissimilar metal Ni-based cast superalloy K418 and alloy steel 42CrMo. *Opt Lasers Eng.* <https://doi.org/10.1016/j.optlaseng.2007.03.004>
11. Li Y, Liu Y, Yang J (2020) First principle calculations and mechanical properties of the intermetallic compounds in a laser welded steel/aluminum joint. *Opt Laser Technol.* <https://doi.org/10.1016/j.optlastec.2019.105875>
12. Palm M (1997) The Al-Cr-Fe system-Phases and phase equilibria in the Al-rich corner. *J Alloys Compd.* [https://doi.org/10.1016/S0925-8388\(96\)02719-3](https://doi.org/10.1016/S0925-8388(96)02719-3)
13. Quazi MM, Ishak M, Fazal MA, et al (2020) Current research and development status of dissimilar materials laser welding of titanium and its alloys. *Opt Laser Technol* 126:106090. <https://doi.org/10.1016/j.optlastec.2020.106090>
14. Cao X, Wallace W, Immarigeon J-P, Poon C (2003) Research and Progress in Laser Welding of Wrought Aluminum Alloys. II. Metallurgical Microstructures, Defects, and Mechanical Properties. *Mater Manuf Process* 18:23–49.

- <https://doi.org/10.1081/AMP-120017587>
15. Huang H, Yang L-M, Bai S, Liu J (2014) Femtosecond fiber laser welding of dissimilar metals. *Appl Opt*. <https://doi.org/10.1364/ao.53.006569>
  16. Yang J, Li YL, Zhang H (2016) Microstructure and mechanical properties of pulsed laser welded Al/steel dissimilar joint. *Trans Nonferrous Met Soc China (English Ed)*. [https://doi.org/10.1016/S1003-6326\(16\)64196-1](https://doi.org/10.1016/S1003-6326(16)64196-1)
  17. Pardal G, Meco S, Dunn A, et al (2017) Laser spot welding of laser textured steel to aluminium. *J Mater Process Technol* 241:24–35. <https://doi.org/10.1016/j.jmatprotec.2016.10.025>
  18. Meco S, Pardal G, Ganguly S, et al (2013) Overlap conduction laser welding of aluminium to steel. *Int J Adv Manuf Technol* 67:647–654. <https://doi.org/10.1007/s00170-012-4512-6>
  19. Meco S, Ganguly S, Williams S, McPherson N (2019) Design of laser welding applied to T joints between steel and aluminium. *J Mater Process Technol* 268:132–139. <https://doi.org/10.1016/j.jmatprotec.2019.01.003>
  20. Meco S, Cozzolino L, Ganguly S, et al (2017) Laser welding of steel to aluminium: Thermal modelling and joint strength analysis. *J Mater Process Tech* 247:121–133. <https://doi.org/10.1016/j.jmatprotec.2017.04.002>
  21. Sierra G, Peyre P, Deschauxbeaume F, et al (2007) Steel to aluminium key-hole laser welding. *Mater Sci Eng A* 447:197–208. <https://doi.org/10.1016/j.msea.2006.10.106>
  22. Torkamany MJ, Malek Ghaini F, Poursalehi R, Kaplan AFH (2016)

- Combination of laser keyhole and conduction welding: Dissimilar laser welding of niobium and Ti-6Al-4V. *Opt Lasers Eng.* <https://doi.org/10.1016/j.optlaseng.2015.11.001>
23. Suder WJ, Williams SW (2012) Investigation of the effects of basic laser material interaction parameters in laser welding. *J Laser Appl* 24:032009. <https://doi.org/10.2351/1.4728136>
  24. Coroado J, Meco S, Williams S, et al (2017) Fundamental understanding of the interaction of continuous wave laser with aluminium. <https://doi.org/10.1007/s00170-017-0702-6>
  25. Banat D, Ganguly S, Meco S, Harrison P (2020) Application of high power pulsed nanosecond fibre lasers in processing ultra-thin aluminium foils. *Opt Lasers Eng* 129:. <https://doi.org/10.1016/j.optlaseng.2020.106075>
  26. Williams S, Suder W (2011) Use of fundamental laser material interaction parameters in laser welding. *CLEO 2011 - Laser Sci to Photonic Appl* 1–2
  27. John A (2015) Dissimilar welding of stainless steel to aluminium thin sheet using nano-second pulsed fibre laser. Dissertation, Cranfield University
  28. Alsaidi M, Caballero A, Eze S, et al (2015) Study of laser metal interaction for pulsed nanosecond fibre laser. Dissertation, Cranfield University
  29. Coroado J, Ganguly S, Suder W, et al (2021) Selection of parameters in nanosecond pulsed wave laser micro-welding. *Int J Adv Manuf Technol.* <https://doi.org/10.1007/s00170-021-07251-8>
  30. TRUMPF (2014) 100W G4 pulsed fibre laser specification interface manual.

TRUMPF Lasers UK Ltd, Southampton

31. Chmelickova H, Ctvrtlik R, Stranyanek M (2004) Pulsed laser welding of thin metals. In: Proc. SPIE 5445, Microwave and Optical Technology. pp 356–359
32. aalco (2019) Aluminium Alloy 5251 - H22 Sheet and Plate properties. [http://www.aalco.co.uk/datasheets/Aluminium-Alloy-5251-H22-Sheet-and-Plate\\_150.ashx](http://www.aalco.co.uk/datasheets/Aluminium-Alloy-5251-H22-Sheet-and-Plate_150.ashx). Accessed 1 Oct 2019
33. aalco (2019) Stainless Steel - Austenitic - 304L properties. [http://www.aalco.co.uk/datasheets/Stainless-Steel-14301-Sheet-and-Plate-Quarto-Plate--CPP-Plate\\_343.ashx](http://www.aalco.co.uk/datasheets/Stainless-Steel-14301-Sheet-and-Plate-Quarto-Plate--CPP-Plate_343.ashx). Accessed 1 Oct 2019
34. Suder W (2011) Study of fundamental parameters in hybrid laser welding. Dissertation, Cranfield University
35. Meco S (2016) Joining of steel to aluminium alloys for advanced structural applications. Dissertation, Cranfield University
36. British Standard Institution (2001) BS EN ISO 14273:2001 Specimen dimensions and procedure for shear testing resistance spot , seam and embossed projection welds. London
37. Qiu R, Iwamoto C, Satonaka S (2009) Interfacial microstructure and strength of steel/aluminum alloy joints welded by resistance spot welding with cover plate. *J Mater Process Technol* 209:4186–4193. <https://doi.org/10.1016/j.jmatprotec.2008.11.003>
38. Olsen FO (2009) Hybrid Laser Arc Welding. In: Hybrid Laser-Arc Welding, 1st ed. CRC Press, pp 270–295

39. Lee SJ, Nakamura H, Kawahito Y, Katayama S (2014) Effect of welding speed on microstructural and mechanical properties of laser lap weld joints in dissimilar Al and Cu sheets. *Sci Technol Weld Join* 19:111–118. <https://doi.org/10.1179/1362171813Y.0000000168>
40. Massalski T (1986) *Binary Alloy Phase Diagrams*, American S. Williams, Jr. W. Scott, Metals Park, Ohio
41. Xiao R, Zhang X (2014) Problems and issues in laser beam welding of aluminum-lithium alloys. *J Manuf Process* 16:166–175. <https://doi.org/10.1016/j.jmapro.2013.10.005>
42. Indhu R, Divya S, Tak M, Soundarapandian S (2018) Microstructure development in Pulsed Laser Welding of Dual Phase Steel to Aluminium Alloy. In: *Procedia Manufacturing*